reduced due to the hydrophobicity that limits cell contacts with the surface.

However, we wanted to verify toxicity related to the incorporation of GO solubilized with a polar solvent into PCL material. As shown in Fig. 4(b), the toxicity toward VERO cells of the DMEM conditioned with the PCL-GO scaffolds for 7 days is not significantly higher compared to cells treated with DMEM conditioned with PCL scaffold. In other words, even after 7 days of scaffold submersion in DMEM, there is no significant release of toxic molecules in the medium.

However, in Fig. 4(c), from fluorescence images of cells labeled with calcein and propidium iodide, a local cytotoxic effect of PCL-GO scaffolds is visible: cells in red, i.e., dead cells, are distributed along scaffolds borders as shown also in Fig. 4(d) by brightfield image of the sample. The red signal from dead cells disappears with increased distance. Consequently, the scaffold inhibits cell adhesion and has a local inhibition of growth but is not toxic toward the cells grown in the same petri since conditioned DMEM toxicity is negligible [Fig. 4(b)].

The advantages of decreased cell adhesion in PCL-GO include minimizing the risk of biofouling, a common issue in biomedical applications, especially in the surgical environment, where bacterial contamination is facilitated. However, it is important to control long-term cell adhesion to ensure scaffold biodegradability and population over time, paramount in promoting successful tissue regeneration and minimizing the risk of necrotic infections. To understand the process and to verify the long-term effect of local cytotoxicity, we repeatedly washed the scaffolds with different protocols.

In Fig. 4(e), a comparison of washing with PBS or PBS+ethanol is shown for PCL and PCL-GO. We observe, with the increase in the number of washes, a notable increase in cell attachment on the scaffold, especially with washes with PBS+ethanol. The use of ethanol, in which the dichloromethane (DCM) is soluble, allows for a quicker removal of DCM residues. After three washes, the cell adhesion is markedly increased, and the PCL-GO can increase cell attachment five times more than PCL, as reported in the literature for other graphene-enriched materials.[59] Therefore, the residuals of polar solvents persist on GO due to its ability to act as a surfactant.

*In vivo*, the removal of DCM and the change of the surface will likely occur in an environment rich in salts, plasma proteins, and nutrients. To simulate this, we repeatedly washed the scaffold with DMEM growth medium. After 1 week of washing, the bioconductivity of PCL-GO scaffolds reaches that of PCL [Fig. 4(f)].

Accordingly, red dead cells are not visible around the grid in fluorescence images of VERO cells grown on DMEM washed scaffolds [Figs. 4(g) and 4(h)].

This phenomenon can be explained by a change in the hydrophilicity after repeated washings of scaffolds as shown in Figs. 4(i) and 4(j) with contact angle measurement. We therefore hypothesize, after washes, a combined effect of (i) a reduced amount of solvent, (ii) an increase in the hydrophilicity, and (iii) the rough morphology of PCL-GO observed with surface characterization in Fig. 2. We point out that this result is significant for the 3D printing of graphene and GO and more, in general, for the 3D printing of DCM-solubilized PCL scaffolds that also gain a certain degree of hydrophilicity after washings [Fig. 4(e)].

We then 3D-printed scaffolds directly into petri dishes using different scaffold heights.

We observed a sudden detachment from the surface for PCL scaffolds, probably since the PCL-GO is more hydrophobic or due to the more homogeneous nature of PCL-GO composite that improves scaffold adhesion to plastic [Fig. 5(a)].

For PCL-GO, we prepared a scaffold having different heights: a gradient from 50 to 100 $\mu m$ [Fig. 5(b)] or constant height 200 $\mu m$ [Fig. 5(c)] and washed surfaces with DMEM multiple times. Interestingly, we observed a cell distribution according to height: while cells attached easily to flat scaffold surfaces [Fig. 5(d)], in other cases, we observed that the higher the height, the lower the cellular adhesion [Figs. 5(e) and 5(f)], with a complete evading of the grid area for 200 $\mu m$ high scaffolds [Fig. 5(f)]. We hypothesize, due to the absence of dead cells in Figs. 5(d) and 5(e), an effect of DCM removal proportional to the area exposed to DMEM washing. This would allow *in vivo* to foresee the cellular distribution according to the height of the surface of the scaffold coatings/device thickness, allowing to increase the cellular adhesion in precise scaffold areas.

This phenomenon can also be exploited to 3D print grids directly into petri dishes for cell confinement in experiments, like wound healing or microfluidics assays. The grid can then be removed, and the islet of cells can be obtained on petri surfaces, as shown as proof of concept in Figs. 5(g) and 5(h).

## Limiting infections on implants: Antibacterial effects of PCL-GO scaffolds

Surgical infections can arise through two primary routes: contiguously and hematogenously. Contiguous contamination occurs during the implantation process itself, where microorganisms from the surrounding environment may inadvertently come into contact with the scaffold. Hematogenous spread, on the other hand, involves the introduction of infectious agents via the bloodstream. While the body's natural defenses typically prevent such systemic infections, certain factors, such as compromised immune function or preexisting infections, can increase the risk. Therefore, meticulous attention to both aseptic techniques during surgery and the design of implantable materials that discourage microbial adhesion is crucial in minimizing the potential for surgical site infections.

To test the antibacterial properties of PCL and PCL-GO scaffolds, *E. coli* or *S. aureus* cells were deposited on scaffolds and let interact in a controlled environment as described in the Methods section. The results in terms of CFU collected from surfaces are shown in Fig. 6(a).

On fresh surfaces, on PCL-GO, there is a reduction of ∼81% concerning the number of *E. coli* cells and a ∼69% reduction of *S. aureus* cell number compared to PCL, demonstrating PCL-GO as an excellent candidate for infection control during the initial implantation, which is fundamental for infections derived from surgical environment. IR treatment of PCL-GO surfaces does not significantly improve the antibacterial efficacy of PCL-GO at this stage.

The long-term efficacy of surfaces has been tested after repeated washing, to assess whether the antibacterial effect is preserved over a prolonged time *in vivo*. As reported for eukaryotic cells, the washing of the surfaces induces modifications that improve hydrophilicity and consequently bacterial adhesion [Fig. 6(b)]. However, thanks to the IR adsorptive properties of PCL-GO, the antibacterial effect is restored after 30 s of treatment both for *E. coli* and *S. aureus*. Representative images of CFU plates and SEM images of *E. coli* grown on surfaces are shown in Fig. 6(c).

The addition of GO on surfaces has been often reported to induce antibacterial properties: GO is, indeed, known to affect the
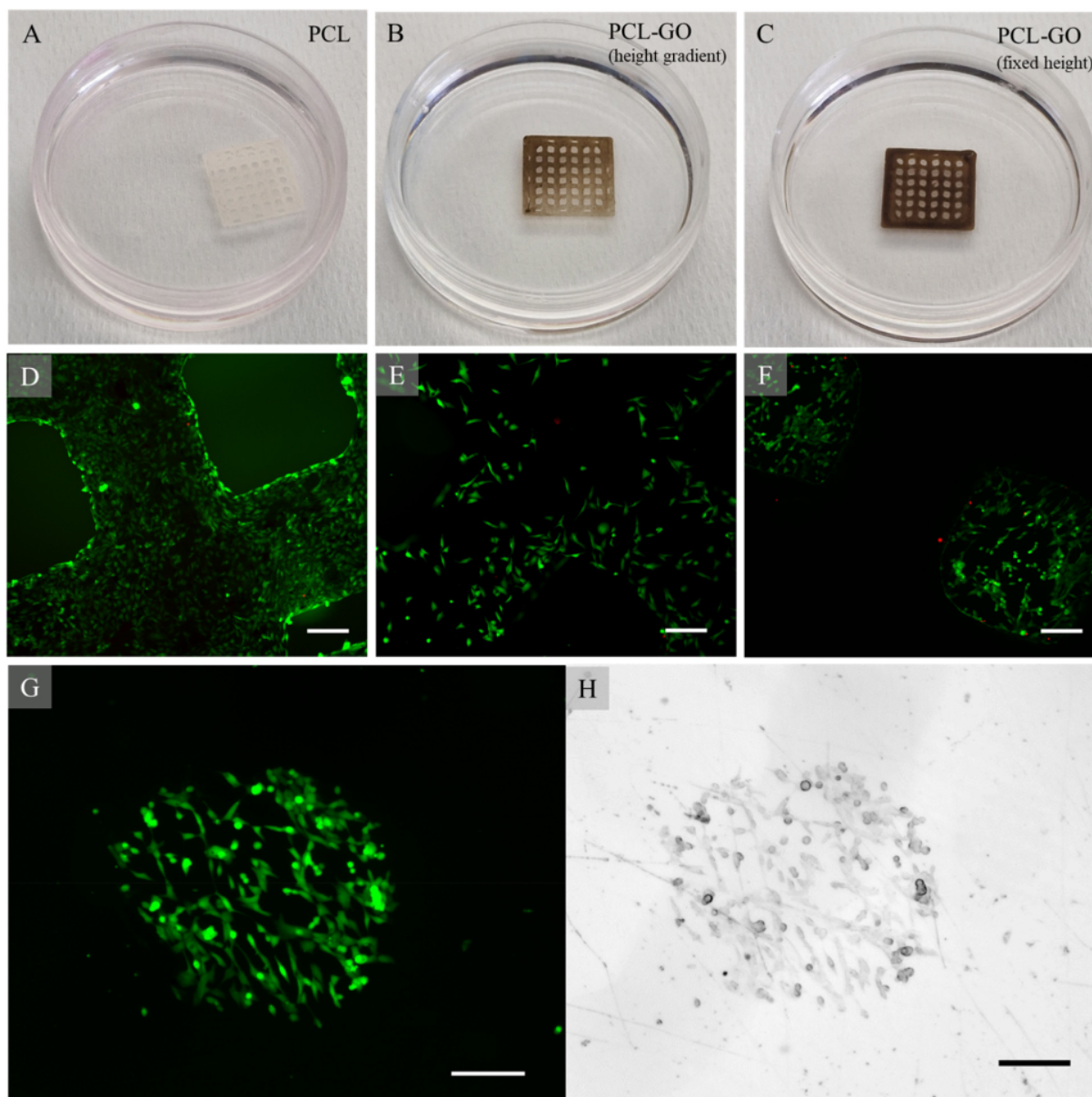
**FIG. 5.** Images of PCL grids (a) or PCL-GO grids (b) and (c) printed at different heights. Fluorescence images of grids areas with 50 (d), 100 (e), or 200 $\mu$m height (f). Fluorescence (g) and brightfield (h) representative images of cells confined in the area defined by the PCL-GO grid. The scale bar is 100 $\mu$m.

cell membrane and cell wall of microorganisms by producing ROS and through physical demolition and chemical oxidation, resulting in microbial death.[60] This is, however, a phenomenon well comprised in soluble GO experiments.[61,62] On scaffolds, the antibacterial efficacy of GO is more likely proportional to the amount of GO surface available to interact with bacterial cells.[63,64] In this case, we hypothesize that as for cells, the DCM residuals are responsible for the antibacterial effects that are lost after repeated washes. Even if

the antibacterial efficacy would gradually be lost *in vivo*, the IR absorptive properties of GO can be used to reduce any long-term infection that might occur after implantation as demonstrated in Fig. 6(c).

## CONCLUSIONS

The demand for versatile materials in medicine is evident across a wide spectrum of applications, ranging from supporting structures
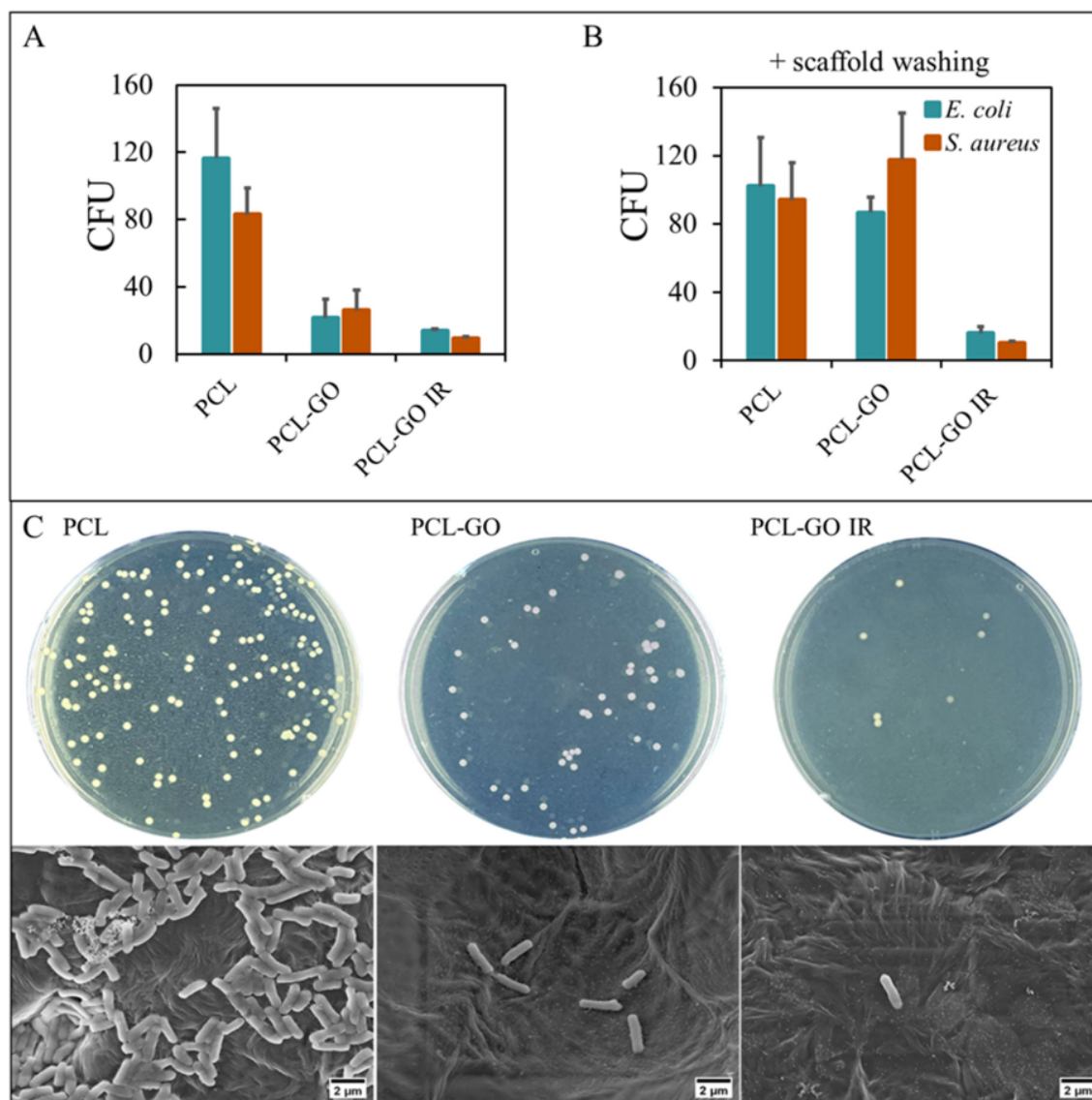
04 March 2024 09:31:24

**FIG. 6.** Antibacterial effects of PCL and PCL-GO scaffolds, with or without IR irradiation, on *E. coli* or *S. aureus* cells seeded on scaffolds (a). After scaffold washing, the CFUs have been measured and reported in (b), the CFU/ml is CFU$*10^5$ according to the dilution used for plating. Representative images of CFU plates and SEM imaging for *E. coli* (c).

like bones to delicate interactions with soft tissues. A significant challenge in medical settings is the occurrence of biofouling, which involves the unwanted buildup and proliferation of microorganisms on implanted materials. In addition to the need to counter infections, it is imperative to integrate scaffolds *in vivo* over time. This integration is essential for enabling tissue regeneration and ensuring the proper functioning of biomedical implants.

In this work, we demonstrate that the addition of a small percentage of GO to PCL allows to 3D print scaffolds with multiple functionalities. GO improves the mechanical performance of PCL and infers IR

absorption properties.[17,65] The added GO dramatically changes the surface features due to the heat conductivity improvement during 3D printing and to the retainment of small amounts of DCM that increase hydrophobicity and toxicity of the surface. This is advantageous to prevent fouling from bacteria in the surgical site. It should be pointed out that this toxicity is spatially limited to the few micrometers around the scaffold surface since cells seeded in the proximity of the scaffold grow undisturbedly. When the surface is put in contact with fluids rich in proteins and nutrients, a phenomenon that occurs in all medical devices intended for long-term use *in vivo*, the toxicity is progressively loss

according to the thickness of the scaffold: this allows us to foresee cell attachment behavior and ultimately tissue integration over time. In turn, also antibacterial effects of PCL-GO scaffolds, which are initially very high, are limited when the surface is put in contact with the growth medium for a prolonged period. However, the IR absorption by the scaffold can be used to locally increase temperature and destroy bacterial cells by hyperthermia. This method can ensure bacterial elimination in cases of a secondary infection via hematogenous spreading, as an example.

We highlight that the low cell attachment feature of PCL-GO can be also exploited to create confined cell areas for experiments like wound healing or invasion assays, and co-cultures to replicate tissue structures by modulating scaffold height and/or composition.

The increase in hydrophilicity obtained for PCL and PCL-GO after repeated washings represents a time-controlled low-cost simple strategy compared to protein coating, cold plasma treatment, and chemical etching. Looking ahead, this research paves the way for the development of advanced biomaterials with diverse applications in tissue engineering and medical device design.

## METHODS

### Materials

The materials used were Alkylamined Graphene Oxide (GO S-921556, Sigma-Aldrich), dichloromethane (DCM, Carlo Erba), ethanol (Carlo Erba), polycaprolactone (PCL, 43–50 kDa, hydroxyl end group. mp 55–65° C, Polysciences, Inc), African green monkey kidney epithelial cells (VERO) (ATCC CCL-81), Dulbecco's Modified Eagle's Medium (DMEM) (Sigma-Aldrich, St. Louis, MO, USA), fetal bovine serum (FBS) EuroClone, streptomycin–penicillin (EuroClone, Milan, Italy), and Murine myoblast C2C12 cells American Type Culture Collection (ATCC). Differentiation medium (DM), made of DMEM, 2% Horse Serum (HS), 100 U/ml penicillin, and 100 $\mu$g/ml streptomycin (EuroClone, Milan, Italy), HEK-Dual$^{TM}$ Null (NF/IL8) cells (Invivogen), RAW 264.7 murine macrophage cell line (ATCC® CRL1469$^{TM}$), CellTiter-Glo® Luminescent Cell Viability Assay (Promega, Madison, WI, USA), E. coli (ATCC 25922), S. aureus (ATCC 29213), LB Broth medium (Sigma-Aldrich), Ph.D.-12 Phage display library kit (New England Biolabs), Propidium Iodide (Sigma-Aldrich), Calcein, AM, cell-permeant dye (Invitrogen$^{TM}$).

### 3D printing

3D printing of scaffolds was performed with a BIO X 3D bioprinter (Cellink). PCL (900 mg) and GO (9 mg) were dissolved in 20 ml of DCM in glass bottles under stirring for 2 h. Then, solutions were mixed under stirring for 1 h, and a GO 1% w/w concentration was obtained after solvent evaporation. The mixture (PCL-GO) was air-dried in large Petri dishes, the produced film was cut into small pieces, and then, it was transferred to a thermoplastic printhead (Cellink, heating capacity of up to 250 °C). The structure of scaffolds was designed using modeled 3D computer graphics and computer-aided design (CAD) software Rhinoceros software (Robert McNeel & Associates). The extrusion-based printing was done using a printhead temperature of 65 °C and a printbed temperature of 25 °C. The extrusion pressure was set at 40 kPa, with a pre-flow of 20 ms and a speed of 22 mm/s, and the nozzle diameter was 200 $\mu$m.

### FT-IR and Raman spectroscopy

The chemical analysis of PCL and PCL-GO was carried out using attenuated total reflectance-Fourier transform infrared spectroscopy (ATR-FTIR) Bruker ALPHA II compact FTIR Spectrometer, equipped with an attenuated total reflection module (Eco-ATR). The material under investigation was directly laid upon the ATR crystal, and the spectra were recorded in the wave number range of 4000–550 cm$^{-1}$, with a resolution of 2 nm. Raman spectra were run at room temperature in backscattering geometry with an inVia Renishaw micro-Raman spectrometer equipped with an air-cooled CCD detector and super-Notch filters. An Ar$^+$ ion laser ($\lambda_{laser} = 514$ nm) was used, coupled to a Leica DLML microscope with a 20× objective. The resolution was 2 cm$^{-1}$, and spectra were calibrated using the 520.5 cm$^{-1}$ line of a silicon wafer. Raman spectra were acquired in several different spots on the surface of the samples. For GO, PCL, and PCL-GO composite, each spectrum was acquired with 1% of power, 10 s of spectral acquisition, and 20 scans.

### Mechanical properties

Mechanical testing of samples was performed to retrieve tensile strength (TS), elongation at break (EB), and elastic modulus (EM) using 3D printed dog-bone-shaped specimens and a mechanical analyzer (UniVert CellScale system, Canada). The grip separation was 20 mm, and the speed rate was 1 mm/s until breaking. At least three samples for each condition were used.[66]

### IR photothermal properties

To assess the photothermal properties of 3D printed materials, samples were irradiated under an 808 nm (diode Laser Ever, China) for different time spans at a power density of 1.6 W/cm$^2$. A thermal imaging camera (Xi400, Optris) was used to record the sample temperature. All tests were performed in triplicate.

### Wettability

Contact angle measurements were performed on each material surface using the drop shape analysis method[66] using 10 $\mu$l of deionized water and the instrument described in the literature.[67]

### Morphological characterization of samples

To perform imaging, samples were first cleaned to remove any contaminants or debris using ethanol and then rinsed with distilled water to remove any residual ethanol. The samples were deposited on sterile mica slides and air-dried overnight.

Atomic force microscopy (AFM) was performed with a NanoWizard II (JPK Instruments AG, Berlin, Germany) in contact mode. The images were acquired using silicon cantilevers with high aspect-ratio conical silicon tips (CSC37 Mikro-Masch, Tallinn, Estonia) characterized by an end radius of about 10 nm, a half conical angle of 20°, and a spring constant of 0.6 N/m. Scan areas of 10 × 10 $\mu$m$^2$ were imaged.

The surface roughness of all samples was evaluated using the software JPK SPM Data Processing. Three areas were imaged with AFM for each sample, and the roughness was measured in terms of both the arithmetical mean deviation of the assessed profile (Ra) and of root mean squared (Rq).

Scanning electron microscopy (SEM) was performed to evaluate 3D-printed scaffold morphology. All the samples were sputter coated with a layer of 100 nm of gold. Images have been acquired with SEM Supra 25 (Zeiss, Germany) at several magnifications (scale bars are reported on each image). Images were analyzed using FIJI software (National Institutes of Health, Bethesda, MD, USA). For imaging of bacteria cells, samples were fixed in glutaraldehyde (2.5%), dehydrated in ethanol series, and dried and sputter coated with 150 nm of gold.

### Cell cultures, cell adhesion, and toxicity evaluation

VERO, C2C12, RAW 264.7, and HEK cells were cultured in DMEM supplemented with 10% FBS, 2% streptomycin/penicillin antibiotics, and in a humidified atmosphere (5% $CO_2$, 37 °C). To investigate cell attachment on PCL and PCL-GO, VERO, C2C12, HEK, and RAW cells were cultured on PCL and PCL-GO supports, and viability was assessed after 72 h by using CellTiter-Glo® Luminescent Cell Viability Assay according to manufacturer's instructions. Plastic was used as control. To measure the cell viability, CellTiter-Glo was added to each well with a volume equal to culture medium and shaken for 2 min in an orbital shaker to induce cell lysis. Plates were incubated at room temperature for 10 min before recording luminescence using a Cytation 3 Cell Imaging Multi-Mode Reader (Cytation 3, Biotek, USA).

### Antibacterial effects

Samples were tested for their antibacterial performance. *E. coli* ATCC 25922 or *S. aureus* ATCC 29213 adhesion on surfaces was quantified using the colony counting method as previously reported.[68] Bacteria were inoculated in a Lennox LB Broth at 37 °C overnight. Afterward, 250 $\mu$l of cell suspension was subcultured in 250 ml of LB, and then cells were harvested at the exponential growth phase and diluted in PBS. PCL and PCL-GO samples were incubated with 50 $\mu$l of bacteria suspension diluted in PBS at a concentration of $10^5$ CFU/ml and incubated for 3 h. At the end of the incubation, the samples were washed and vortexed in PBS to recover cells from the surface. The resulting solution was cultured on LB Agar plates and incubated at 37 °C overnight. After incubation, the CFUs were quantified. For IR treatment, scaffolds were exposed to IR light at a power density of 1.6 $W/cm^2$ for 30 s. Each experiment was repeated in triplicate.

### Phage adhesion and phage display

A library of random peptides, 12 amino acids long displayed on the minor coat protein, gene III, of the bacteriophage M13 was used for phages experiments (Ph.D.-12 Phage display library kit). *E. coli* host strain K12ER2738 was used for plating and propagation into LB/tetracycline medium plates, using overnight incubation at 37 °C. A polyethylene 96-wells plate was used for the panning procedure with different scaffolds PCL or PCL-GO surfaces. Each well was filled with 300 $\mu$l blocking buffer (0.1 M NaHCO$_3$ pH 8.6) and incubated for 1 h at 4 °C; then, the wells were rapidly washed six times with 300 $\mu$l TBST (tris buffered saline-tween). 100 $\mu$l of the phage library solution was pipetted into the coated wells and gently rocked for 1 h at room temperature. Unbounded phages were removed by washing with 300 $\mu$l TBST ten times. To elute the bounded phages, 100 $\mu$l of 0.2 M glycline-HCl (pH 2.2) and 1 mg/ml BSA were added to each well and incubated for 8 min upon gently rocking; then, the pH of the eluate

was neutralized with 15 $\mu$l 1M Tris-HCl (pH 9.1). Subsequently, the eluted phage solution was tittered using 200 $\mu$l *E. coli* strain ER2738, grown in LB medium at 37 °C. After that, the infected cells were transferred to culture tubes containing melted top agar, vortexed, and poured on LB/IPTG/Xgal plates for incubation at 37 °C. After the third round of biopanning, predominant scaffold-binding selective phages were isolated and sequenced.[69]

## AUTHOR DECLARATIONS
### Conflict of Interest

The authors have no conflicts to disclose.

### Ethics Approval

Ethics approval is not required.

### Author Contributions

G. Friggeri and I. Moretti contributed equally to this work.

**G. Friggeri:** Data curation (equal); Formal analysis (equal); Investigation (equal); Methodology (equal); Writing – original draft (equal). **I. Moretti:** Data curation (equal); Formal analysis (equal); Investigation (equal); Methodology (equal); Writing – original draft (equal). **F. Amato:** Data curation (equal); Formal analysis (equal); Methodology (equal); Writing – original draft (equal). **A. G. Marrani:** Data curation (equal); Formal analysis (equal); Resources (equal); Supervision (equal); Writing – original draft (equal). **F. Sciandra:** Data curation (equal); Formal analysis (equal); Resources (equal); Writing – original draft (equal). **S. G. Colombarolli:** Data curation (equal); Formal analysis (equal). **A. Vitali:** Formal analysis (equal); Funding acquisition (equal). **S. Viscuso:** Data curation (equal); Formal analysis (equal); Visualization (equal). **Alberto Augello:** Conceptualization (equal); Data curation (equal); Formal analysis (equal); Investigation (equal); Methodology (equal); Writing – original draft (equal). **L. Cui:** Investigation (equal); Methodology (equal). **G. Perini:** Data curation (equal); Investigation (equal); Writing – original draft (equal). **M. De Spirito:** Resources (equal); Supervision (equal); Validation (equal); Writing – review & editing (equal). **M. Papi:** Funding acquisition

04 March 2024 09:31:24

(equal); Resources (equal); Supervision (equal); Validation (equal); Writing – review & editing (equal). **V. Palmieri:** Conceptualization (equal); Funding acquisition (equal); Investigation (equal); Project administration (equal); Resources (equal); Supervision (equal); Validation (equal); Writing – original draft (equal); Writing – review & editing (equal).

## DATA AVAILABILITY

The data that support the findings of this study are available from the corresponding authors upon reasonable request.

## REFERENCES

[1] J. L. Gerardo-Nava, J. Jansen, D. Günther, L. Klasen, A. L. Thiebes, B. Niessing et al., "Transformative materials to create 3D functional human tissue models in vitro in a reproducible manner," Adv. Healthcare Mater. **12**, 2301030 (2023).

[2] X. Deng, M. Gould, and M. A. Ali, "Fabrication and characterisation of melt-extruded chitosan/keratin/PCL/PEG drug-eluting sutures designed for wound healing," Mater. Sci. Eng. C **120**, 111696 (2021).

[3] P. Grossen, D. Witzigmann, S. Sieber, and J. Huwyler, "PEG-PCL-based nano-medicines: A biodegradable drug delivery system and its application," J. Control Release **260**, 46–60 (2017).

[4] N. Siddiqui, S. Asawa, B. Birru, R. Baadhe, and S. Rao, "PCL-based composite scaffold matrices for tissue engineering applications," Mol. Biotechnol. **60**, 506–532 (2018).

[5] S.-R. Son, N.-T. B. Linh, H.-M. Yang, and B.-T. Lee, "*In vitro* and *in vivo* evaluation of electrospun PCL/PMMA fibrous scaffolds for bone regeneration," Sci. Technol. Adv. Mater. **14**, 015009 (2013).

[6] Z. Yin, D. Li, Y. Liu, S. Feng, L. Yao, X. Liang et al., "Regeneration of elastic cartilage with accurate human-ear shape based on PCL strengthened biodegradable scaffold and expanded microtia chondrocytes," Appl. Mater. Today **20**, 100724 (2020).

[7] A. Ghaee, S. Bagheri-Khoulenjani, H. A. Afshar, and H. Bogheiri, "Biomimetic nanocomposite scaffolds based on surface modified PCL-nanofibers containing curcumin embedded in chitosan/gelatin for skin regeneration," Composites, Part B **177**, 107339 (2019).

[8] E. M. J. Lin, C. L. Lay, G. S. Subramanian, W. S. Tan, S. S. J. Leong, L. C. H. Moh et al., "Control release coating for urinary catheters with enhanced released profile for sustained antimicrobial protection," ACS Appl. Mater. Interfaces **13**, 59263–59274 (2021).

[9] D. S. Chan, N. Fnais, I. Ibrahim, S. J. Daniel, and J. Manoukian, "Exploring polycaprolactone in tracheal surgery: A scoping review of in-vivo studies," Int. J. Pediatr. Otorhinolaryngol. **123**, 38–42 (2019).

[10] A. J. Guerra, P. Cano, M. Rabionet, T. Puig, and J. Ciurana, "3D-printed PCL/PLA composite stents: Towards a new solution to cardiovascular problems," Materials **11**, 1679 (2018).

[11] K. M. Ali and B. M. A. Al-Jaff, "Source and antibiotic susceptibility of gram-negative bacteria causing superficial incisional surgical site infections," Int. J. Surg. Open **30**, 100318 (2021).

[12] L. Liu, Y. Zhang, C. Li, J. Cao, E. He, X. Wu et al., "Facile preparation PCL/modified nano ZnO organic-inorganic composite and its application in antibacterial materials," J. Polym. Res. **27**, 78 (2020).

[13] C. M. Magin, S. P. Cooper, and A. B. Brennan, "Non-toxic antifouling strategies," Mater. Today **13**, 36–44 (2010).

[14] M. M. Hossain and V. R. Lokasani, "Improving the hydrophobicity of polymers through surface texturing," in Conference Proceedings Society of Plastics Engineers, 2021.

[15] V. Palmieri, M. De Spirito, and M. Papi, "Nanofeatures of orthopedic implant surfaces," Future Med. **16**, 1733–1736 (2021).

[16] G. Perini, A. Rosenkranz, G. Friggeri, D. Zambrano, E. Rosa, A. Augello et al., "Advanced usage of Ti$_3$C$_2$T$_x$ MXenes for photothermal therapy on different 3D breast cancer models," Biomed. Pharmacother. **153**, 113496 (2022).

[17] V. Palmieri, F. Sciandra, M. Bozzi, M. De Spirito, and M. Papi, "3D graphene scaffolds for skeletal muscle regeneration: Future perspectives," Front. Bioeng. Biotechnol. **8**, 383 (2020).

[18] A. K. Geim and K. S. Novoselov, "The rise of graphene," Nat. Mater. **6**, 183–191 (2007).

[19] Y. Zhang, Y.-W. Tan, H. L. Stormer, and P. Kim, "Experimental observation of the quantum Hall effect and Berry's phase in graphene," Nature **438**, 201–204 (2005).

[20] K. S. Novoselov, A. K. Geim, S. V. Morozov, D. Jiang, M. I. Katsnelson, I. V. Grigorieva et al., "Two-dimensional gas of massless Dirac fermions in graphene," Nature **438**, 197–200 (2005).

[21] J.-H. Chen, C. Jang, S. Xiao, M. Ishigami, and M. S. Fuhrer, "Intrinsic and extrinsic performance limits of graphene devices on SiO$_2$," Nat. Nanotechnol. **3**, 206–209 (2008).

[22] K.-J. Tielrooij, J. C. W. Song, S. A. Jensen, A. Centeno, A. Pesquera, A. Zurutuza Elorza et al., "Photoexcitation cascade and multiple hot-carrier generation in graphene," Nat. Phys. **9**, 248–252 (2013).

[23] A. H. C. Neto, F. Guinea, N. M. R. Peres, K. S. Novoselov, and A. K. Geim, "The electronic properties of graphene," Rev. Mod. Phys. **81**, 109 (2009).

[24] C. Lee, X. Wei, J. W. Kysar, and J. Hone, "Measurement of the elastic properties and intrinsic strength of monolayer graphene," Science **321**, 385–388 (2008).

[25] V. Palmieri, E. A. Dalchiele, G. Perini, A. Motta, M. De Spirito, R. Zanoni et al., "Biocompatible *N*-acetyl cysteine reduces graphene oxide and persists at the surface as a green radical scavenger," Chem. Commun. **55**, 4186 (2019).

[26] F. Amato, G. Perini, G. Friggeri, A. Augello, A. Motta, L. Giaccari et al., "Unlocking the stability of reduced graphene oxide nanosheets in biological media via use of sodium ascorbate," Adv. Mater. Interfaces **10**, 2300105 (2023).

[27] A. T. Smith, A. M. LaChance, S. Zeng, B. Liu, and L. Sun, "Synthesis, properties, and applications of graphene oxide/reduced graphene oxide and their nanocomposites," Nano Mater. Sci. **1**, 31–47 (2019).

[28] B. Lesiak, G. Trykowski, J. Tóth, S. Biniak, L. Kövér, N. Rangam et al., "Chemical and structural properties of reduced graphene oxide—Dependence on the reducing agent," J. Mater. Sci. **56**, 3738–3754 (2021).

[29] P. Bellet, M. Gasparotto, S. Pressi, A. Fortunato, G. Scapin, M. Mba et al., "Graphene-based scaffolds for regenerative medicine," Nanomaterials **11**, 404 (2021).

[30] A. Savchenko, R. T. Yin, D. Kireev, I. R. Efimov, and E. Molokanova, "Graphene-based scaffolds: Fundamentals and applications for cardiovascular tissue engineering," Front. Bioeng. Biotechnol. **9**, 797340 (2021).

[31] L. Feng, W. Li, J. Ren, and X. Qu, "Electrochemically and DNA-triggered cell release from ferrocene/$\beta$-cyclodextrin and aptamer modified dualfunctionalized graphene substrate," Nano Res. **8**, 887–899 (2015).

[32] H. J. Yoon, A. Shanker, Y. Wang, M. Kozminsky, Q. Jin, N. Palanisamy et al., "Tunable thermal-sensitive polymer-graphene oxide composite for efficient capture and release of viable circulating tumor cells," Adv. Mater. **28**, 4891–4897 (2016).

[33] Z. Dai, Y. Wang, L. Liu, X. Liu, P. Tan, Z. Xu et al., "Hierarchical graphene-based films with dynamic self-stiffening for biomimetic artificial muscle," Adv. Funct. Mater. **26**, 7003–7010 (2016).

[34] W. Li, J. Wang, J. Ren, and X. Qu, "3D graphene oxide-polymer hydrogel: Near-infrared light-triggered active scaffold for reversible cell capture and on-demand release," Adv. Mater. **25**, 6737–6743 (2013).

[35] W. Li, J. Wang, J. Ren, and X. Qu, "Near-infrared upconversion controls photocaged cell adhesion," J. Am. Chem. Soc. **136**, 2248–2251 (2014).

[36] N. Mauro, S. E. Drago, G. Cavallaro, and G. Giammona, "Near-infrared, light-triggered, on-demand anti-inflammatories and antibiotics release by graphene oxide/elecrospun PCL patch for wound healing," C—Journal of Carbon Research. **5**(4), 63 (2019).

[37] L. Ferroni, C. Gardin, F. Rigoni, E. Balliana, F. Zanotti, M. Scatto et al., "The impact of graphene oxide on polycaprolactone PCL surfaces: Antimicrobial activity and osteogenic differentiation of mesenchymal stem cell," Coatings **12**, 799 (2022).

[38] S. Yıldırım, T. T. Demirtaş, C. A. Dinçer, N. Yıldız, and A. Karakeçili, "Preparation of polycaprolactone/graphene oxide scaffolds: A green route combining supercritial CO$_2$ technology and porogen leaching," J. Supercrit. Fluids **133**, 156–162 (2018).

[39] Y. Li, C. Liao, and S. C. Tjong, "Synthetic biodegradable aliphatic polyester nanocomposites reinforced with nanohydroxyapatite and/or graphene oxide for bone tissue engineering applications," Nanomaterials **9**, 590 (2019).

[40]B. M. Bijonowski, *Spatiotemporal Regulation of Cell–Cell Adhesions*, edited by M. Anwar, Z. Farooq, R. A. Rather, M. Tauseef, and T. Heinbockel (IntechOpen, Rijeka, 2021).

[41]A. Seyedsalehi, L. Daneshmandi, M. Barajaa, J. Riordan, and C. T. Laurencin, "Fabrication and characterization of mechanically competent 3D printed polycaprolactone-reduced graphene oxide scaffolds," Sci. Rep. **10**, 22210 (2020).

[42]P. Haji Mohammadi Gohari, M. Haghbin Nazarpak, and M. Solati-Hashjin, "The effect of adding reduced graphene oxide to electrospun polycaprolactone scaffolds on MG-63 cells activity," Mater. Today Commun. **27**, 102287 (2021).

[43]W. Wang, J.-X. Chen, Y. Hou, P. Bartolo, and W.-H. Chiang, "Investigations of graphene and nitrogen-doped graphene enhanced polycaprolactone 3D scaffolds for bone tissue engineering," Nanomaterials **11**, 929 (2021).

[44]P. R. Lopes Nalesso, W. Wang, Y. Hou, L. Bagne, A. T. Pereira, J. V. Helaehil *et al.*, "*In vivo* investigation of 3D printed polycaprolactone/graphene electroactive bone scaffolds," Bioprinting **24**, e00164 (2021).

[45]C. Zhang, D. M. Dabbs, L.-M. Liu, I. A. Aksay, R. Car, and A. Selloni, "Combined effects of functional groups, lattice defects, and edges in the infrared spectra of graphene oxide," J. Phys. Chem. C **119**, 18167–18176 (2015).

[46]S. Guo, S. Garaj, A. Bianco, and C. Ménard-Moyon, "Controlling covalent chemistry on graphene oxide," Nat. Rev. Phys. **4**, 247–262 (2022).

[47]F. Amato, A. Motta, L. Giaccari, R. Pasquale, F. Scaramuzzo, R. Zanoni *et al.*, "One-pot carboxyl enrichment fosters water-dispersibility of reduced graphene oxide: A combined experimental and theoretical assessment," Nanoscale **5**, 893 (2023).

[48]T. Elzein, M. Nasser-Eddine, C. Delaite, S. Bistac, and P. Dumas, "FTIR study of polycaprolactone chain organization at interfaces," J. Colloid Interface Sci. **273**, 381–387 (2004).

[49]O. Hartman, C. Zhang, E. L. Adams, M. C. Farach-Carson, N. J. Petrelli, B. D. Chase *et al.*, "Biofunctionalization of electrospun PCL-based scaffolds with perlecan domain IV peptide to create a 3-D pharmacokinetic cancer model," Biomaterials **31**, 5700–5718 (2010).

[50]M. Ermeydan, E. Cabane, P. Hass, J. Koetz, and I. Burgert, "Fully biodegradable modification of wood for improvement of dimensional stability and water absorption properties by poly($\varepsilon$-caprolactone) grafting into the cell walls," Green Chem. **16**, 3313–3321 (2014).

[51]A. Baranowska-Korczyc, A. Warowicka, M. Jasiurkowska-Delaporte, B. Grześkowiak, M. Jarek, B. Maciejewska *et al.*, "Antimicrobial electrospun poly $\varepsilon$-caprolactone scaffolds for gingival fibroblast growth," RSC Adv. **6**, 19647 (2016).

[52]P. Taddei, A. Tinti, and G. Fini, "Vibrational spectroscopy of polymeric biomaterials," J. Raman Spectrosc. **32**, 619–629 (2001).

[53]V. Palmieri, F. Amato, A. G. Marrani, G. Friggeri, G. Perini, A. Augello *et al.*, "Graphene oxide-mediated copper reduction allows comparative evaluation of oxygenated reactive residues exposure on the materials surface in a simple one-step method," Appl. Surf. Sci. **615**, 156315 (2023).

[54]W. Kai, Y. Hirota, L. Hua, and Y. Inoue, "Thermal and mechanical properties of a poly($\varepsilon$-caprolactone)/graphite oxide composite," J. Appl. Polym. Sci. **107**, 1395–1400 (2008).

[55]C. Wan and B. Chen, "Poly($\varepsilon$-caprolactone)/graphene oxide biocomposites: Mechanical properties and bioactivity," Biomed. Mater. **6**, 55010 (2011).

[56]N. Akhigan, N. Najmoddin, H. Azizi, and M. Mohammadi, "Zinc oxide surface-functionalized PCL/graphene oxide scaffold: Enhanced mechanical and antibacterial properties," Int. J. Polym. Mater. Polym. Biomater. **72**, 1423–1433 (2023).

[57]V. Palmieri, M. D. Spirito, and M. Papi, "Graphene-based scaffolds for tissue engineering and photothermal therapy," Nanomedicine **15**, 1411–1417 (2020).

[58]R. Dwivedi, S. Kumar, R. Pandey, A. Mahajan, D. Nandana, D. S. Katti *et al.*, "Polycaprolactone as biomaterial for bone scaffolds: Review of literature," J. Oral Biol. Craniofacial Res. **10**, 381–388 (2020).

[59]J. M. Unagolla and A. C. Jayasuriya, "Enhanced cell functions on graphene oxide incorporated 3D printed polycaprolactone scaffolds," Mater. Sci. Eng. C **102**, 1–11 (2019).

[60]S. F. Melo, S. C. Neves, A. T. Pereira, I. Borges, P. L. Granja, F. D. Magalhães *et al.*, "Incorporation of graphene oxide into poly($\varepsilon$-caprolactone) 3D printed fibrous scaffolds improves their antimicrobial properties," Mater. Sci. Eng. C **109**, 110537 (2020).

[61]V. Palmieri, F. Bugli, M. C. Lauriola, M. Cacaci, R. Torelli, G. Ciasca *et al.*, "Bacteria meet graphene: Modulation of graphene oxide nanosheet interaction with human pathogens for effective antimicrobial therapy," ACS Biomater. Sci. Eng. **3**, 619–627 (2017).

[62]F. De Maio, V. Palmieri, A. Salustri, G. Perini, M. Sanguinetti, M. De Spirito *et al.*, "Graphene oxide prevents mycobacteria entry in macrophages through extracellular entrapment," Nanoscale Adv. **1**, 1421 (2019).

[63]M. Papi, V. Palmieri, F. Bugli, M. De Spirito, M. Sanguinetti, C. Ciancico *et al.*, "Biomimetic antimicrobial cloak by graphene-oxide agar hydrogel," Sci. Rep. **6**, 12 (2016).

[64]V. Palmieri, M. Barba, L. Di Pietro, S. Gentilini, M. C. Braidotti, C. Ciancico *et al.*, "Reduction and shaping of graphene-oxide by laser-printing for controlled bone tissue regeneration and bacterial killing," 2D Mater. **5**, 15027 (2017).

[65]V. Palmieri, W. Lattanzi, G. Perini, A. Augello, M. Papi, and M. De Spirito, "3D-printed graphene for bone reconstruction," 2D Mater. **7**, 022004 (2020).

[66]F. De Maio, E. Rosa, G. Perini, A. Augello, B. Niccolini, F. Ciaiola *et al.*, "3D-printed graphene polylactic acid devices resistant to SARS-CoV-2: Sunlight-mediated sterilization of additive manufactured objects," Carbon **194**, 34–41 (2022).

[67]R. Chalise, A. Niroula, P. Shrestha, B. Paudel, D. Subedi, and R. Khanal, "A low-cost goniometer for contact angle measurements using drop image analysis: Development and validation," AIP Adv. **13**, 85123 (2023).

[68]A. Rosenkranz, G. Perini, J. Y. Aguilar-Hurtado, D. F. Zambrano, B. Wang, B. Niccolini *et al.*, "Laser-mediated antibacterial effects of few- and multi-layer $Ti_3C_2T_x$ MXenes," Appl. Surf. Sci. **567**, 150795 (2021).

[69]S. G. Colombarolli, A. Vitali, and F. Sciandra, *Extracellular Vesicle Molecular Profiling for Diagnostic Purposes: An Application of Phage Display Technology BT - Peptide Microarrays: Methods and Protocols*, edited by M. Cretich and A. Gori (Springer US, New York, 2023), pp. 237–247.